Journal of Energy Storage 20 (2018) 140–152

Contents lists available at ScienceDirect

Journal of Energy Storage

journal homepage: www.elsevier.com/locate/est

Study of supercritical power plant integration with high temperature thermal energy storage for flexible operation

Decai Li, Jihong Wang*

School of Engineering, University of Warwick, Coventry CV4 7AL, UK

ARTICLE INFO

Keywords:
Supercritical coal-fired power plant
High temperature thermal storage
Frequency responses
Dynamic systems

ABSTRACT

The paper presents the recent research in study of the strategies for the power plant flexible operation to serve the requirement of grid frequency control and load balance. The study aims to investigate whether it is feasible to bring the High Temperature Thermal Storage (HTTS) to the thermal power plant steam-water cycle, to identify the suitable thermal charge and discharge locations in the cycle and to test how the HTTS integration can help support grid operation via power plant dynamic mathematical modelling and simulation. The simulation software named SimuEngine is adopted and a 600 MW supercritical coal-fired power plant model is implemented onto the software platform. Three HTTS charging strategies and two HTTS discharging strategies are proposed and tested via the simulation platform. The simulation results show that it is feasible to extract steam from the steam turbine to charge the HTTS, and to discharge the stored thermal energy back to the power generation processes. With the integration of the HTTS charge and discharge processes, the power plant simulation model is also connected to a simplified GB (Great Britain) grid model. Then the study is extended to test the improved capability of the plant flexible operation in supporting the responses to the grid load demand changes. The simulation results demonstrate that the power plant with HTTS integration has faster dynamic responses to the load demand changes and, in turn, faster response to grid frequency services.

1. Introduction

The current balance between power generation and load demand is mainly managed through regulating the output of fossil fuel power plants. With the rapid increase of power generation from renewable energy, fossil fuel power plants are required to play more important role in maintaining load balance and providing the grid frequency control service as they are considered as dispatchable power generation units. Fossil fuel power plants are now required to work more flexibly, responding faster with more frequent start-ups or shut-downs for maintaining power network stability; this can cause two serious issues: low plant efficiency and low load factors. To address these issues, it is essential to explore new technologies and operation strategies. The paper reports the recent research progress in the integration of High Temperature Thermal Storage (HTTS) with a supercritical boiler power plant to enable the power plant cycle to operate more flexibly while maintaining its thermal efficiency.

The concept of using Thermal Energy Storage (TES) for regulating the thermal plant power generation was initially reported in [1] decades ago. Several studies [2,3] were recently reported on incorporation of TES into Combined Heat and Power (CHP) generations, in which TES is used to regulate the balance of the demand for heat and electricity supply. A report indicates that a high temperature latent heat TES unit is to be built in an operating cogeneration plant in Saarland, Germany [4]. In this planned power station, HTTS produces superheated steam to industrial customers in an emergency. Also, many studies have been reported in the area of solar thermal power plant integration with TES, in which TES plays an important role to time shifting of energy delivery in an economic way [5–9]. Besides, the study of a combined-cycle gas turbine power plant combined with TES in order to improve the plant flexibility is presented in [10]. Moreover, Wojcik [11] presented a feasibility study of TES integration with a 375 MW subcritical oil-fired conventional power plant for flexible operation.

For the supercritical coal-fired power plant, the flexible operation is the rapid power response capability for satisfying frequency control. The boiler turbine coordinated control is a widely adopted control strategy to regulate power generation in thermal power plants. However, the plant dynamic response is slow due to the large time delay of the energy transfer from the fuel supply to the water-steam loop [12]. A revised water fuel ratio control strategy was proposed by Wang to enhance the peak shaving capacity of supercritical coal-fired power plant [13]. Besides, Zhao proposed a method for improving the

* Corresponding author.
E-mail address: jihong.wang@warwick.ac.uk (J. Wang).

https://doi.org/10.1016/j.est.2018.09.008
Received 26 April 2018; Received in revised form 10 September 2018; Accepted 13 September 2018
Available online 22 September 2018

Nomenclature

Abbreviations

CHP	Combined Heat and Power
GB	Great Britain
HTF	Heat Transfer Fluid
HTTS	High Temperature Thermal Storage
IPTB	Intermediate Pressure Turbine
LPTB	Low Pressure Turbine
TES	Thermal Energy Storage

Symbols

C_{CND1}	Minimum heat transfer coefficient of saturated section
C_{CND2}	Heat transfer coefficient of saturated section
C_{DRN1}	Minimum heat transfer coefficient of drain cooling section
C_{DRN2}	Heat transfer coefficient of drain cooling section
C_{DS1}	Minimum heat transfer coefficient of superheat section
C_{DS2}	Heat transfer coefficient of superheat section
C_{pm}	Specific heat of water
$E_{kinetic}$	Stored kinetic energy of a synchronous machine
D	Load response $kg{\cdot}m^2$
f_0	Grid normal frequency Hz
h	Enthalpy $kJ{\cdot}kg^{-1}$
h'	Saturated water enthalpy $kJ{\cdot}kg^{-1}$
J	System inertia
K_a, K_{da}	Heat dissipation to the atmosphere, Heat dissipation of drain cooling sectik$J{\cdot}K^{-1}{\cdot}s^{-1}$
K_f	Pipedirty influence coefficient
$\overline{K}_{Lcond}$	Condensatelevel influence coefficient when pipe exposes in steam
$\overline{K}_{LDRN}$	Condensatelevel influence coefficient when pipe submerge in water
$K_{LD\,sup}$	Superheatsection coefficient
K_{wa}	Heat dissipation of water $kJ{\cdot}K^{-1}{\cdot}s^{-1}$
L	Enthalpy of phase change $kJ{\cdot}kg^{-1}$
M_m	Totalquality of pipe kg
M_{PCM}	Mass of PCM
P	Pressure Pa
ΔP	Pressure head of inlet and outlet, Pa
$Q_{storage}$	Stored thermal energy$J$
r_0	Resistance factor when valve opening is k, and temperature is $0°C$
r_{00}	Resistance factor when valve opening is 1, and temperature is $0°C$
s	Entropy$kJ{\cdot}kg^{-1}{\cdot}K^{-1}$
S_i	Normal power of the i-th generation unit
S_{rated}	Nominal power rating
T	Temperature
T_m	Atmosphere temperature$°C$
T_s	Temperature in shell side $°C$
V	Volume m^3
V_s, V_w	Valid volume of shell, Valid volume of pipe m^3
W	Water/steam flow rate $kg{\cdot}s^{-1}$
ρ	Density $kg{\cdot}m^{-3}$
ρ_s, ρ_w	Density in shell side, Density of water $kg{\cdot}m^{-3}$

Subscript

a	Atmosphere
de, dl	Drain water entrance, Drain water
lk	Pipe leakage
s	Steam
sat	Saturation
se	Steamentrance
w	Water
we, wl	Feed water entrance, Feed water outlet

operational flexibility of a supercritical coal-fired power plant by regulation extraction steam of high pressure heaters [14]. In summary, the previous studies focused on improving the control strategies to achieve the operational flexibility of power plant.

On the other hand, the thermal inertia of the once-through boiler is smaller than natural circulation boiler, so the capability of offering primary frequency reserve is decreased. This motivates to utilize the HTTS in the supercritical coal-fired power plant to provide an

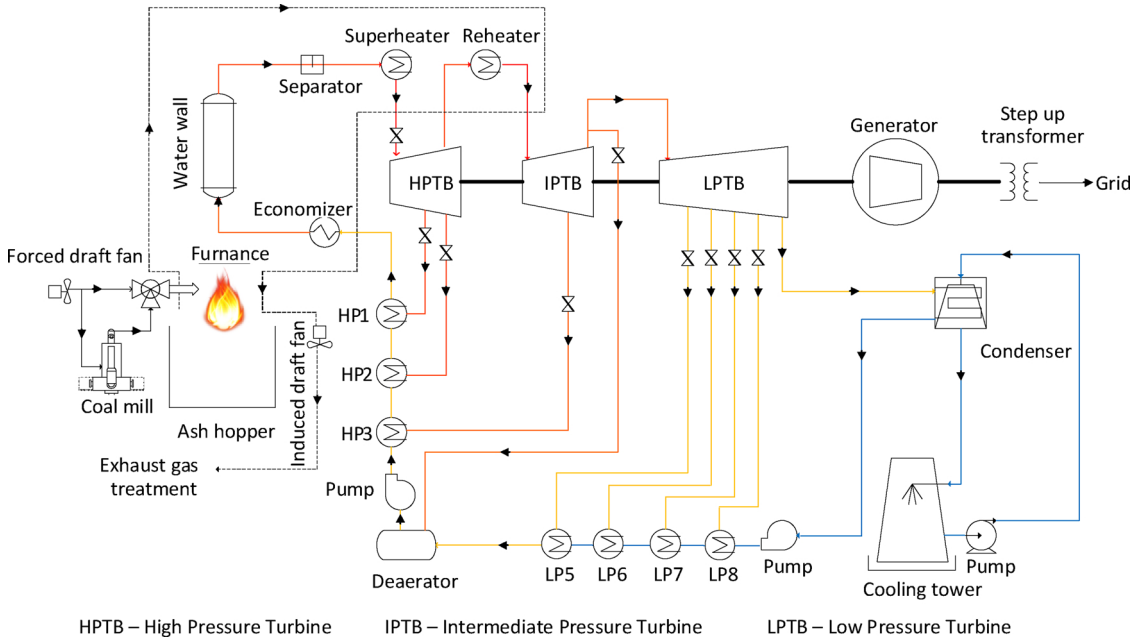

Fig. 1. Schematic of typical supercritical boiler coal-fired power plant.

additional thermal reserve. From the knowledge of the authors, no studies on supercritical coal-fired power plant integration with HTTS have been reported publically.

This paper examines the feasible ways to integrate an HTTS unit into the water-steam cycle of a supercritical coal-fired power plant. The HTTS stores the thermal energy taken from steam while the electricity demand is low and release the stored thermal energy while the electricity demand is high. This study analyses various potential HTTS integration strategies, the viable operation temperature range, charging and discharging options. With HTTS integration, further study is conducted to investigate how the HTTS integration can help the plant operation to provide better support to power grid frequency control. The main contributions of the paper include: the feasible strategies are proposed for HTTS charging and discharging processes; the HTTS integration processes are analysed from energy and exergy balance perspectives; further study is conducted to demonstrate HTTS integration for improving the performance of grid frequency control.

2. Supercritical coal-fired power plant modelling and the simulation platform

Supercritical coal-fired power plants have a higher thermal efficiency than subcritical coal-fired power plants due to their higher operation temperature (500–600 ℃) and pressure (24–26 MPa). The schematic diagram of a typical supercritical coal-fired power plant is shown in Fig. 1. From the figure, it can be seen that there is no steam drum in its water-steam cycle to buffer the steam (thermal energy), which leads to less flexibility in operation compared with subcritical power plants.

In practice, it is almost impossible to test HTTS integration on a real power plant without considerable feasibility pre-study and off-line test. The mathematical modelling and simulation is the approach used in this study which starts with building a power plant dynamic process model. SimuEngine was initially developed by Tsinghua University, China and then further exploited in the University of Warwick, UK. SimuEngine is a digital 600 MW supercritical coal-fired power plant modelling and simulation platform coded in FORTRAN language, which is built on the following fundamental mathematical models of the plant.

The models for steam heaters are derived with respect to the principle of mass and energy conservation, with convergence parameters. The fluid mass change is determined by the mass flow in and out of the junction point of observation and can be described by mass conservation equation [15]:

$$V_s\frac{d\rho_s}{dt} = W_{se} + W_{de} + W_{lk} - W_{dl}, \tag{1}$$

where, V_s is the volume of shell side, ρ_s is the steam density in shell side, W_{se} is the steam entrance mass flow rate, W_{de} is the drain water entrance mass flow rate, W_{lk} is the pipe leakage mass flow rate, and W_{dl} is the drain water mass flow rate.

With the hypotheses that the momentum balance is neglected and the pressure is assumed to be constant in the steam water heater, the energy change at each observation junction is governed by the energy conservation equation [16]:

$$V\rho\frac{dh}{dt} = Q - W\Delta h, \tag{2}$$

where, the left side of the equation is the enthalpy (h) change rate of the working fluid in time domain, Q is the heat transfer rate of the working fluid, and $W\Delta h$ is the enthalpy change of the working fluid in space domain.

The heat transfer rate of the working fluid is determined by the temperature difference between the two working fluids, and the heat transfer coefficient (U). Heat transfer rate of the superheat section can be written as:

$$Q_{DS} = U_{DS}(T_{se} - T_{wl}), \tag{3}$$

where, U_{DS} is the heat transfer coefficient of the superheat section, which can be obtained by:

$$U_{DS} = (C_{DS1} + C_{DS2}W^{we})W^{se}K_f K_{LD\,\mathrm{sup}}. \tag{4}$$

Heat transfer rate in the saturation section or condensation section is therefore described by:

$$Q_{CND} = U_{CND}(T_{sat} - \frac{T_{we} + T_{wl}}{2}), \tag{5}$$

where, U_{CND} is the heat transfer coefficient of saturated section, which is calculated by:

$$U_{CND} = (C_{CND1} + C_{CND2}W^{we})T^s K_f \overline{K}_{Lcond}. \tag{6}$$

Heat transfer rate in the drain cooling section is:

$$Q_{DRN} = U_{DRN}(T_{dl} - T_{we}), \tag{7}$$

where, U_{DRN} is the heat transfer coefficient of the drain cooling section, which is:

$$U_{DRN} = (C_{DRN1} + C_{DRN2}W^{we})K_f \overline{K}_{LDRN}. \tag{8}$$

Hence, the energy conservation equation for saturated water in shell side is expressed by:

$$\frac{d}{dt}(\rho_w V_w h_w + \rho_s V_s h_s) = W_{se}(h_{se} - h') + W_{de}(h_{de} - h') + W_{lk}(h_{lk} - h') - U_{DS}(T_{se} - T_{wl}) - U_{CND}(T_{sat} - \tfrac{T_{we}+T_{wl}}{2}) - K_a(T_{sat} - T_a), \tag{9}$$

where, h' is the saturated water enthalpy. Both water and steam exists in the shell side, thus the shell side temperature is calculated by the combination of water section and steam section.

Energy conservation equation for drain cooling section is:

$$\rho_{dl}V_{dl}\frac{dh_{dl}}{dt} = W_{dl}(h' - h_{dl}) - U_{DRN}(T_{dl} - T_{we}) - K_{da}(T_{dl} - T_a). \tag{10}$$

The heater pipe usually is very thin, and the temperature difference between the pipe metal and water is small, therefore, the influence of pipe heat storage can be included into water. With this assumption, the energy conservation equation in water side is derived as:

$$\rho_w V_w\frac{dh_{wl}}{dt} + M_m C_{pm}\frac{dT_m}{dt} = W_{we}(h_{we} - h_{wl}) + U_{DS}(T_{se} - T_{wl}) + U_{CND}(T_{sat} - \tfrac{T_{we}+T_{wl}}{2}) + U_{DRN}(T_{dl} - T_{we}) - K_{wa}(T_{wl} - T_a). \tag{11}$$

All the working fluid flow is connected by a 'flow net' in SimuEngine. Flow net consists of resistance components, power components, inertia nodes and source sink nodes. The task of flow net calculation is to get the pressure of nodes and the flow rate of branches. The flow resistance is used to present the relationship between branch flow pressure drop ΔP and flow rate $G(kg/s)$. The flow resistance factor r is calculated by:

$$r = \frac{\Delta P}{G^2}. \tag{12}$$

The valves are installed in the power plant at various sections to control the flow rate. The flow valve port area is controllable, which results in valve resistance factor changes and the resistance factor is calculated by:

$$r = (1 + \frac{T}{273})r_0(k) = (1 + \frac{T}{273})\frac{r_{00}}{[k \times f(k)]^2}, \tag{13}$$

where, k is the valve opening, and $f(k)$ is a function defined by valve opening and associated coefficients.

Different components of the power plant process are linked via "flow net" which is a realization of recursive steps of calculation for achieving energy balance and mass balance at each connecting note point. The flow net equations are nonlinear, so it is a challenging task to

solve these nonlinear equations. In SimuEngine power plant simulation model, the node pressure method is used, which is to build pressure equations of each node to get linear equations in the flow net. Once the node pressure is calculated, the flow rate of each branches can be calculated by the resistance equation ($rG^2 = \Delta P$). Pure resistance of the flow net is schematically shown in Fig. 2.

Node pressure can be calculated by the equation:

$$P = \sum_{i=1}^{n+m} \frac{P_i}{b_i} \Big/ \sum_{i=1}^{n+m} \frac{1}{b_i}, \tag{14}$$

$$b_i = r_i \times |G_i|,\ i = 1, 2, \cdots, n + m, \tag{15}$$

where, P_i is the pressure of node i, r_i is the resistance factor of branch i, and G_i is the flow rate of branch i.

In the real-time simulation, if the disturbance is small, the solution could be calculated without iteration; if the disturbance is large and cannot be neglected, the iteration is used to improve the accuracy of the solution. All the detailed fundamental physical models of the power plant components and sub-processes are developed via a previous research project and they are implemented onto SimuEngine [17]. The parameters and operation status of the model are tested and verified by using a wide range of real power plant operation data. The details of Simuengine can be found in [18,19], and the model is validated in [18].

Table 1 shows a set of typical water/steam parameters in the measurement points when the supercritical coal-fired power plant works at the rated state, at which this power plant consumes 216.3 tons coal per hour, and generates 600 MW electrical power. With this power plant system model and simulation platform, the feasibility study for HTTS integration is performed. The study is to test the feasible HTTS charge and discharge control strategy to match the need in balancing the grid load demand.

3. Study of HTTS integration strategies

3.1. HTTS charging strategies

The idea proposed in the paper is to extract high temperature steam from the water-steam loop of the power plant which will pass heat exchangers to thermal storage during the off-peak period. In this way, the electrical power output can be regulated via regulating thermal energy output for power generation while maintaining the constant boiler heat generation. This study is to find the answers to the following challenging questions: where the HTTS can be integrated to the power plant cycle and how much thermal energy can be extracted without sacrificing the plant operating performance. Extracting steam from HPTB inlet is not an efficient way for thermal storage because of its high energy quality. Therefore, three heat extraction (HTTS charging) strategies are investigated and two suitable thermal energy extraction locations have been identified, which are IPTB (Intermediate Pressure Turbine) inlet and LPTB (Low Pressure Turbine) inlet. For the plant used for this simulation study, it is found that the steam temperature at IPTB inlet and LPTB inlet are around 565 °C and 355 °C with the pressures around 3.8 MPa and 0.9 MPa, respectively. The simulation results are presented and analysed in the following subsections.

3.1.1. Extracting steam from IPTB and looping the steam back to the condenser

While the steam extraction point is set at the inlet of the IPTB, the high temperature steam will pass a series of heat exchangers for taking out the thermal energy for storage after extraction. The steam will flow into the condenser after the thermal charge process mixing together with the LPTB outlet steam. The schematic of this HTTS charging strategy is shown in Fig. 3.

The amount of steam extraction is controlled by the valve regulations. With different valve openings, the mass flow rate to the turbine and also the power output will be changed. The simulation results of the mass flow rate and the variations of the plant power output with different valve openings are shown in Fig. 4, and the IPTB inlet temperature and pressure are shown in Fig. 5.

The mass flow rate changes will affect the steam temperature and pressures to the turbine. From Fig. 4, it is clear that the charges need to be restricted to a feasible range in order to maintain power plant stable operation. If the extracted steam beyond a critical boundary, the plant output power will continue to decline (valve opening 25%). This is due to the decrease of IPTB and LPTB mass flow rate, which leads to less steam used for feed water preheaters and results in feed water temperature to drop. The simulation study indicates that the maximum rate of steam extraction from the IPTB inlet is 80 kg/s, and the adjustment range of the output power is 13.3% of its rated power.

3.1.2. Extracting steam from LPTB and looping the steam back to the condenser

Instead of the IPTB inlet, the steam extraction at the inlet of LPTB is studied in this section. After the charging process, the steam will flow into the condenser mixing together with the LPTB outlet steam. The schematic of this HTTS charging strategy is shown in Fig. 6.

The simulation results of the mass flow rate and plant power output changes with different valve openings are shown in Fig. 7, and the LPTB inlet temperature and pressure are shown in Fig. 8. Similar to the steam extraction from the IPTB inlet, the simulation study indicates that the maximum rate of steam extraction from the LPTB inlet is 56 kg/s, and the adjustment range of the output power is 6.5% (561 MW).

3.1.3. Extracting steam from IPTB and feeding the steam back at LPTB inlet

The study reported in this section is to test whether the thermal storage can be controlled in order to regulate the steam temperature and pressure after the heat exchanger. When the temperature of the steam is controlled to have the same temperature required by the LPTB inlet, the steam can be fed back to the LPTB directly to mix with the steam coming from IPTB. The schematic of this HTTS charging strategy is shown in Fig. 9.

The simulation results of the mass flow rate and power output associated with different valve openings are shown in Fig. 10.

With various operation status and applying the above HTTS charging strategy, the maximum rate of steam can be extracted from the inlet of IPTB is 174 kg/s, and the adjustment range of the output power is 3.9% (576.5 MW). Excess extraction will lead to the steam pressure drop to lower than the operation pressure required by the IPTB. So this strategy only works with a small range of power regulation. The merit of this strategy is to recycle the steam back to LPTB which will not change the whole system cycle.

3.2. HTTS discharging strategies

During the electricity peak demand period, the stored thermal energy will be discharged back to the water steam loop to increase the total electricity generation. Two strategies have been studied: the first one is to use HTTS to produce high temperature and high pressure steam for steam turbine, considering the temperature of the generated steam is lower than IPTB inlet, therefore it has to be fed into LPTB inlet; another is to use HTTS to preheat the feed water instead of using the

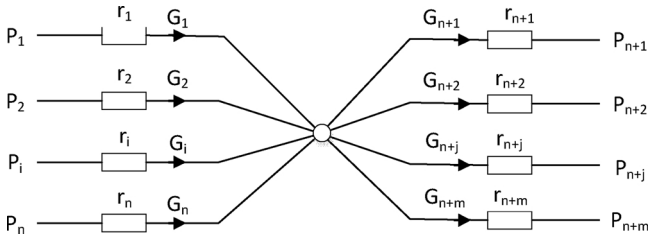

Fig. 2. Flow net diagram for pure resistance branches.

Table 1
Main water/steam parameters in a 600 MW supercritical coal-fired power plant.

	Temperature (°C)	Pressure (MPa)	Flow rate (kg/s)
LP heater inlet	31.96	1.63	351.8
LP heater outlet	107.42	0.62	351.8
HP heater inlet	166.86	27.65	484
HP heater outlet	263.49	27.48	484
Economizer outlet	312.63	27.3	484
Super heater outlet/ HPTB inlet	562.04	25.1	483.9
HPTB outlet	304.72	4.41	445.9
IPTB inlet	565.66	3.8	406.4
IPTB outlet	354.86	0.9	387.2
LPTB inlet	354.86	0.9	309.2

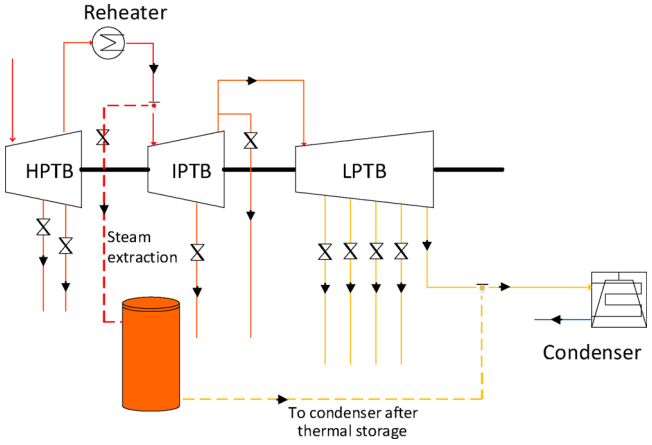

Fig. 3. Schematic of the first HTTS charging strategy.

original preheater. The simulation study for these two strategies is presented and analysed in the following subsections.

3.2.1. Using HTTS to produce additional steam for LPTB

During the HTTS discharging process, part of the feed water flows into the bottom of the HTTS section from the deaerator, evaporates into high temperature steam and is superheated while it rises through the tubes in the HTTS, then it leaves the HTTS as superheated steam. Heat is transferred from the HTTS to the water/steam passing through the tube and increases the temperature of the steam. The steam is then fed to the steam turbine and leads to the increases of the electric power output. As part of water is taken out of the deaerator, more water will need to be pumped into the deaerator in order to maintain the steam flow rate in the HPTB and IPTB. Fig. 11 shows the schematic diagram of the designed HTTS discharging strategy.

Fig. 12 shows the simulation results of plant output with the heat discharge. With the various valve openings, the increased steam flow rate and power output are observed. From the simulation study, the maximum steam flow rate could be increased at the inlet of the LPTB is 72.6 kg/s. As a result, the maximum output power is 644.4 MW, which nearly reaches the plant power output design limit.

3.2.2. Using HTTS to heat the feed water instead of preheater

In a coal-fired supercritical power plant, part of the steam is taken out from the steam turbines to preheat the feed water, as shown in Fig. 1. In this supercritical coal-fired power plant, there are three HP heaters and a group of LP heaters. The steam taken out from the HPTB is used for No.1 and No.2 HP heaters, the extracted steam from the IPTB is used for No.3 HP heater, and the steam taken from LPTB is used for LP heaters as shown in Fig. 1. The amount of the steam extraction is controlled by regulating valve openings; when these valves are closed, more steam will pass through the downstream turbines and produce more power. However, this operation leads to the decrease of the feed water temperature. With the HTTS integration, in order to maintain the feed water temperature, the feed water will bypass the preheaters and flow into HTTS to raise its temperature, and then the stored thermal energy is discharged back to the power generation processes. Simulation results are shown in Fig. 13.

When the valve used to extract steam for No.3 HP heater is closed, the feed water will bypass the No.3 HP heater and heated by the HTTS. So the output power increases to near to 615 MW from 600 MW. When those valves for extracting steam to feed to the LP heater are closed, the feed water will bypass the LP heater and be heated by the HTTS. As a result, the output power increases to around 616.5 MW from 600 MW. When those valves for extracting steam to feed to the LP heater and No.3 HP heater are closed, the feed water will bypass the LP heater and No.3 HP heater and is heated by HTTS. Then the output power increases to 634 MW from 600 MW. This method requires no plant structure changes so it is feasible and cost-effective although the power regulation capability is limited to a small range of power increases.

3.3. Energy and exergy balance analysis

The exergy analysis based on the first and second thermodynamic laws is a tool to provide a clear view of the energy transfer and balance of the power generation process [20]. When power plant achieves its steady state, the stored/released thermal energy and the exergy

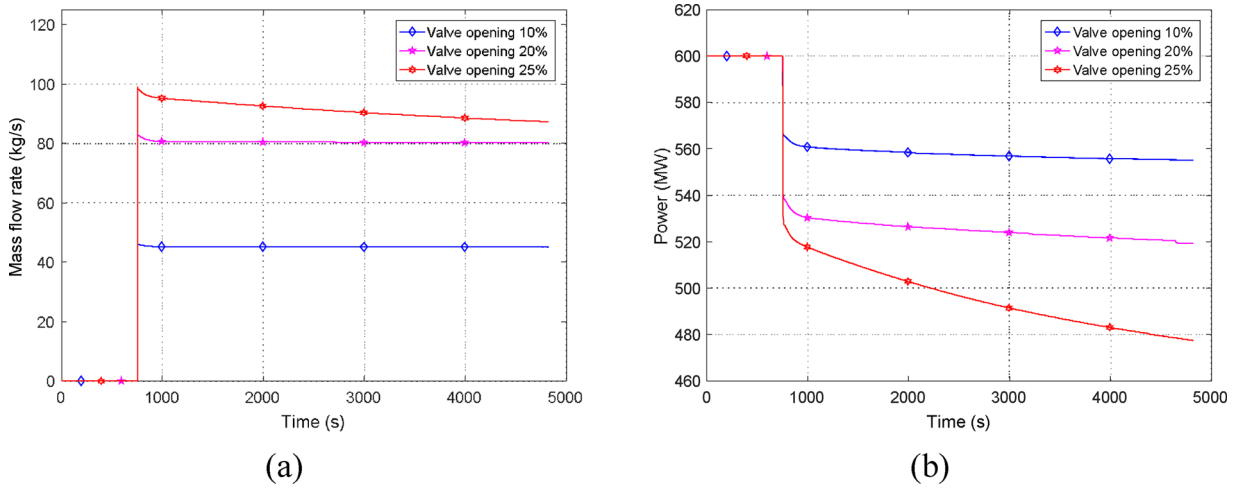

Fig. 4. Relationship of extracted steam from IPTB inlet and output power: (a) Mass flow rate; (b) Output power.

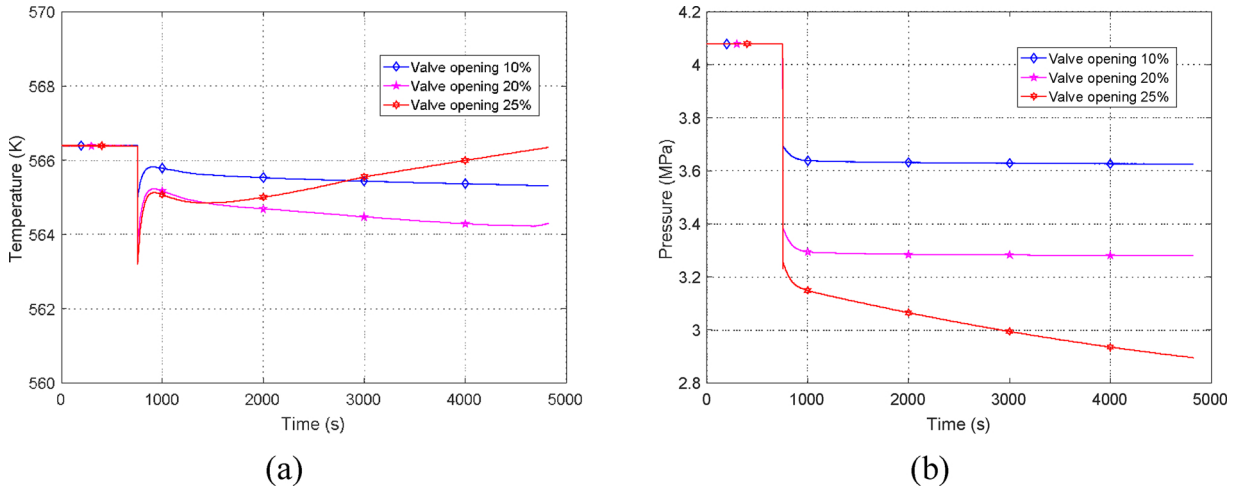

Fig. 5. IPTB inlet: (a) Temperature; (b) Pressure.

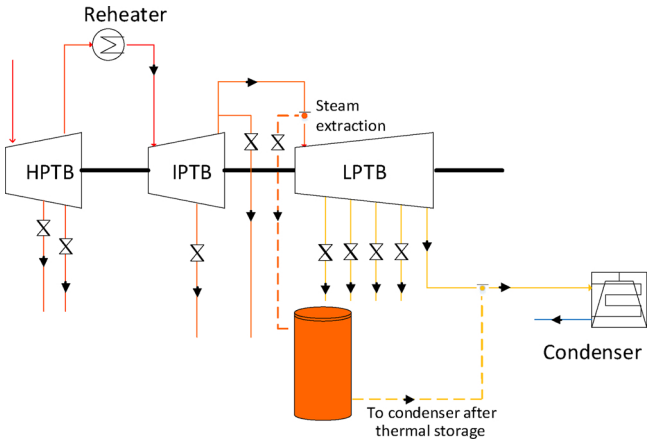

Fig. 6. Schematic of the second HTTS charging strategy.

variation could be calculated.

The stored thermal energy rate ($\dot{E}$) can be calculated by:

$$\dot{E} = \dot{m}(h_{in} - h_{out}), \tag{16}$$

where, $\dot{m}$ is the mass flow rate, subscripts *in* and *out* represent inlet and outlet, respectively. Exergy is the maximum capacity of the energy that can be converted into work. The following equation is used to calculate the specific exergy (ψ) [21]:

$$\psi = h - h_0 - T_0(s - s_0), \tag{17}$$

where, h is the enthalpy, s is the entropy, h_0, T_0, and s_0 are reference enthalpy, temperature and entropy, respectively. The total exergy change rate $\dot{E}_x$ is calculated by [21]:

$$\dot{E}_x = \dot{m}[h - h_0 - T_0(s - s_0)]. \tag{18}$$

The exergy variation rate is given by:

$$\Delta\dot{E}_x = \dot{E}_{x,in} - \dot{E}_{x,out} = \dot{m}[h_{in} - h_{out} - T_0(s_{in} - s_{out})]. \tag{19}$$

Note that the exergy is calculated when T_0 is 298.15 K, P_0 is 101.3 kPa. From the calculation, the stored thermal energy rate and the lost exergy rate for the HTTS charging process is shown in Table 2, which represents the exergy changes of the extracted steam from IPTB inlet and looping back at LPTB inlet. The enthalpy and entropy of IPTB inlet and LPTB inlet are listed in Table 2 for various working conditions, according to the Eqs. (16) and (19) the stored thermal energy and lost exergy are calculated and listed in Table 2.

The released thermal energy rate and the increased exergy rate from the HTTS discharging process is calculated and shown in Table 3, which indicates the additional steam generated by the HTTS energy release for LPTB inlet. It can be seen that from Table 3, in order to increase the exergy of the feed water, the needed thermal energy is nearly triple to the increased exergy. This is due to the entropy has a significant increase during the HTTS discharging process.

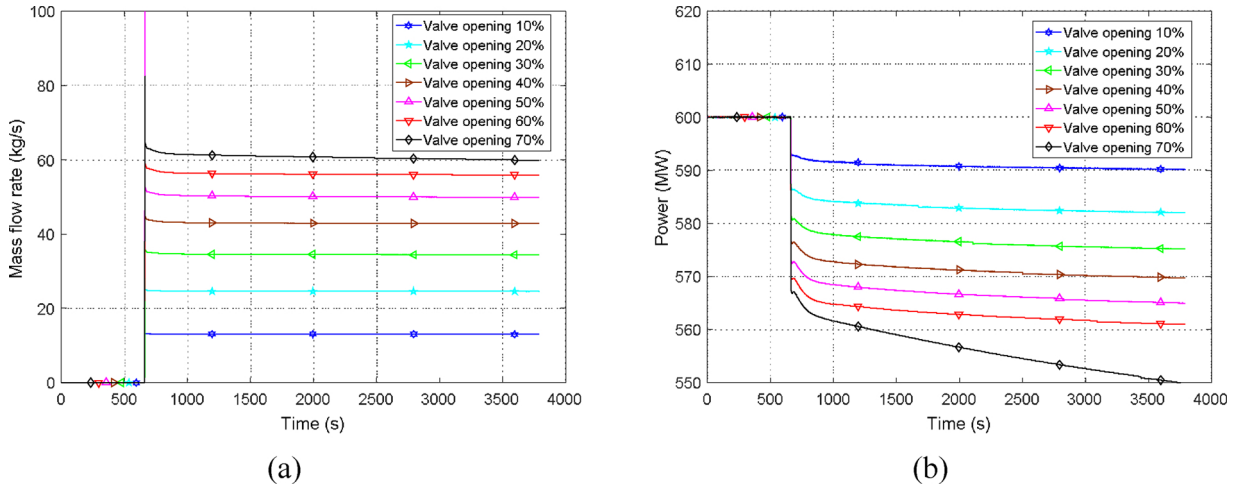

Fig. 7. Relationship of extracted steam from LPTB inlet and output power: (a) Mass flow rate; (b) Output power.

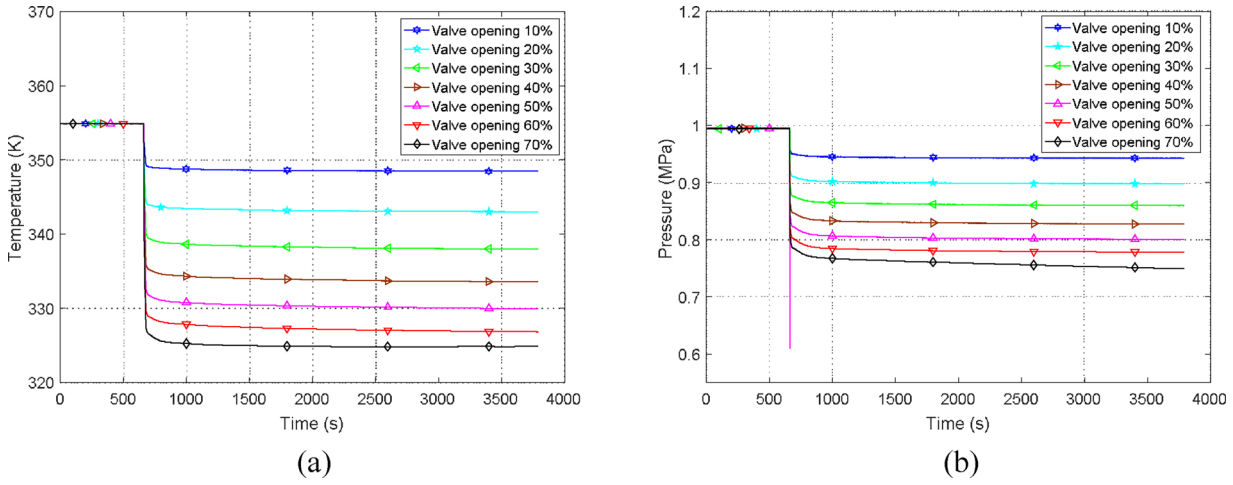

Fig. 8. LPTB inlet: (a) Temperature; (b) Pressure.

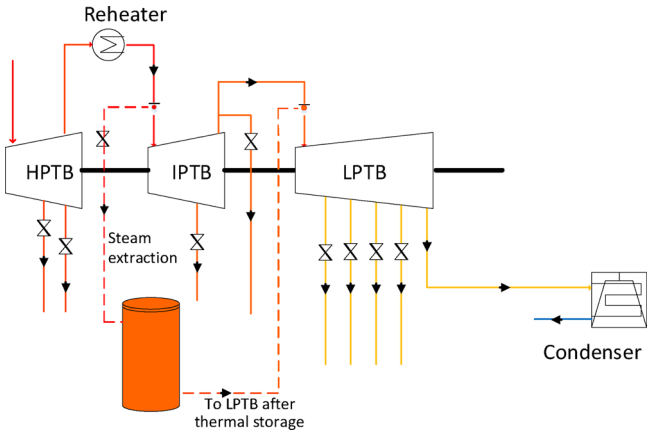

Fig. 9. Schematic of the third HTTS charging strategy.

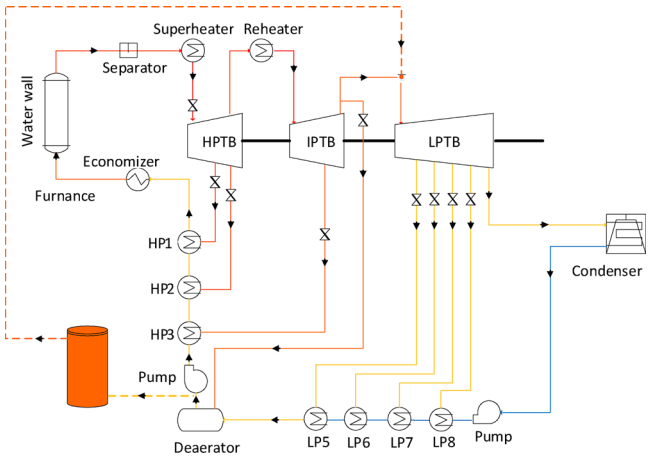

Fig. 11. Schematic of the HTTS discharging strategy.

The plant with HTTS round-trip exergy efficiency can be calculated by [21]:

$$\eta = \frac{W_{out}}{E_{coal}} = \frac{P_1 \cdot t_1 + P_2 \cdot t_2}{\dot{E}_{coal}(t_1 + t_2)}, \tag{20}$$

where, W_{out} is the output electricity, E_{coal} is the exergy of the consumed coal, P_1 and P_2 are the off-peak power and peak power, t_1 and t_2 are the HTTS charging time and discharging time.

The coal specific exergy is given by [21]:

$$\dot{E}_{coal} = \gamma \cdot LHV, \tag{21}$$

where, $\gamma = 1.06$, is the exergy factor, and $LHV = 22MJ/kg$, is the lower heating value [22].

Based on the Tables 2 and 3, if the power plant output power keeps at 590.4 MW for four hours, and then output power increases to

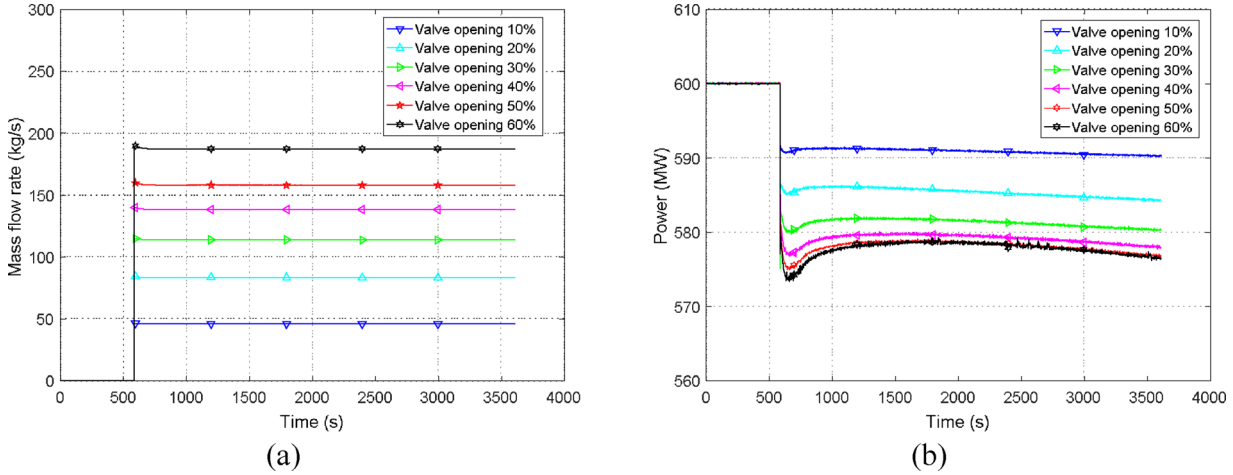

Fig. 10. Relationship of extracted steam from IPTB inlet and output power: (a) Mass flow rate; (b) Output power.

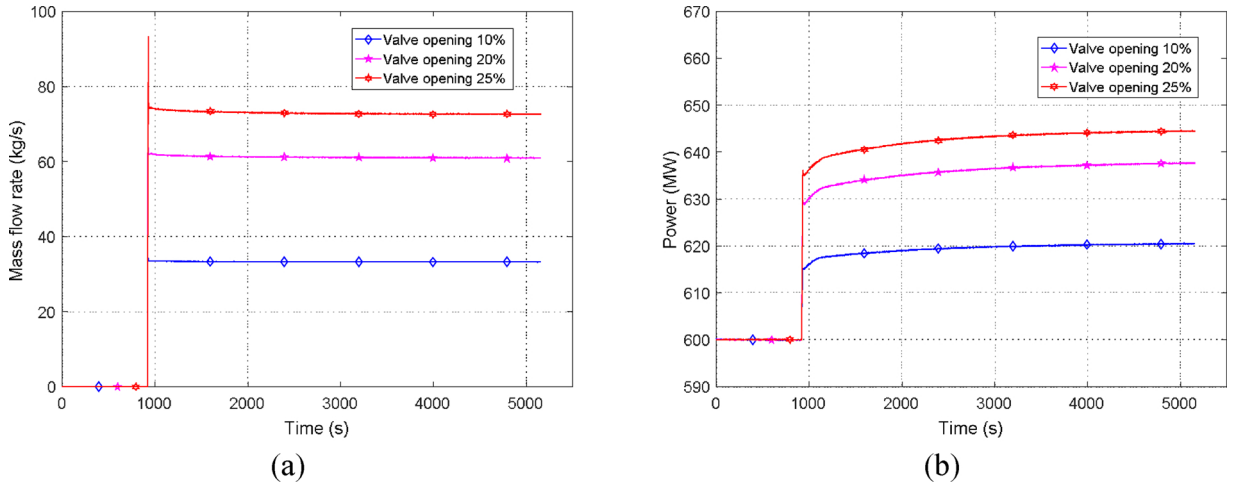

Fig. 12. Relationship of generated steam for LPTB inlet and output power: (a) Mass flow rate; (b) Output power.

620 MW for one hour. According to Eq. (20), the plant round-trip exergy efficiency is 42.56%, in the five hours operation. The plant exergy efficiency is 42.82%, when it works at rated condition.

3.4. High temperature thermal storage

This section presents the designed HTTS model. There are mainly three types of thermal energy storage: sensible heat storage, latent heat storage, and chemical heat storage [6]. Latent heat storage will be used for this study because its energy density is much higher than sensible heat storage and the cost is lower than chemical heat storage [23]. Moreover, as presented by Kuravi, the exergy efficiency of TES can be significantly improved using multiple PCMs compared with a single PCM [6]. Therefore, the designed HTTS model is shown in Fig. 14. The similar design can be found from [6], where the PCMs are different from the proposed model.

The composition of PCMs are: KCl&KF&K_2CO_3, KCl&$ZnCl_2$, KNO_3, LiCl&LiOH and LiNO3&NaNO3&KCl separately arranged along the charging flow direction. Their thermodynamic properties are listed shown in Table 4. For HTTS charging process, the extracted steam flows in the decreasing order of phase change temperature. For the discharging process, the flow direction of HTF is reversed in the increasing order of phase change temperature.

The structure of the above HTTS system consist of two vertical concentric tubes filled with five cascaded PCM layers, as shown in Fig. 15. For each set, the inner tube radius is 0.0215 m, the outer tube radius is 0.043 m, the wall thickness is 0.0015 m, and the height is 15 m (3 m for each PCM layer), as shown in Fig. 16 (a) [25]. The entire HTTS system consists of 6000 sets of such concentric tubes in parallel.

In a cylindrical-coordinate system, the three-dimensional heat conduction equation at point P in Fig. 16 (b) is given by [26]:

$$\rho c_p \frac{\partial T_P}{\partial t} = \frac{1}{r}\frac{\partial}{\partial r}(rk\frac{\partial T}{\partial r}) + \frac{1}{r}\frac{\partial}{\partial \theta}(\frac{k}{r}\frac{\partial T}{\partial \theta}) + \frac{\partial}{\partial z}(k\frac{\partial T}{\partial z}), \tag{22}$$

where, subscript P is the point P in Fig. 16 (b), ρ is the density, k is the heat conduction coefficient, r is the radius, θ is the angle, z is the height. The unique temperature in θ direction is assumed, because the cylinder is a symmetrical structure. Therefore, the two-dimensional heat conduction equation is given by [27]:

$$\rho c_p \frac{\partial T_P}{\partial t} = \frac{1}{r}\frac{\partial}{\partial r}(rk\frac{\partial T}{\partial r}) + \frac{\partial}{\partial z}(k\frac{\partial T}{\partial z}). \tag{23}$$

However, during the phase change, the temperature of PCM maintains at melting temperature. Therefore, the above equation is only used for the calculations under pure solid and liquid conditions. During the melting process, the following equation is used to calculate the enthalpy change [27]:

$$\rho\frac{\partial h_P}{\partial t} = \frac{1}{r}\frac{\partial}{\partial r}(rk\frac{\partial T}{\partial r}) + \frac{\partial}{\partial z}(k\frac{\partial T}{\partial z}). \tag{24}$$

Based on this system, a case study is carried out for the first HTTS charging strategy. The charging HTF mass flow rate is 50 kg/s, and the

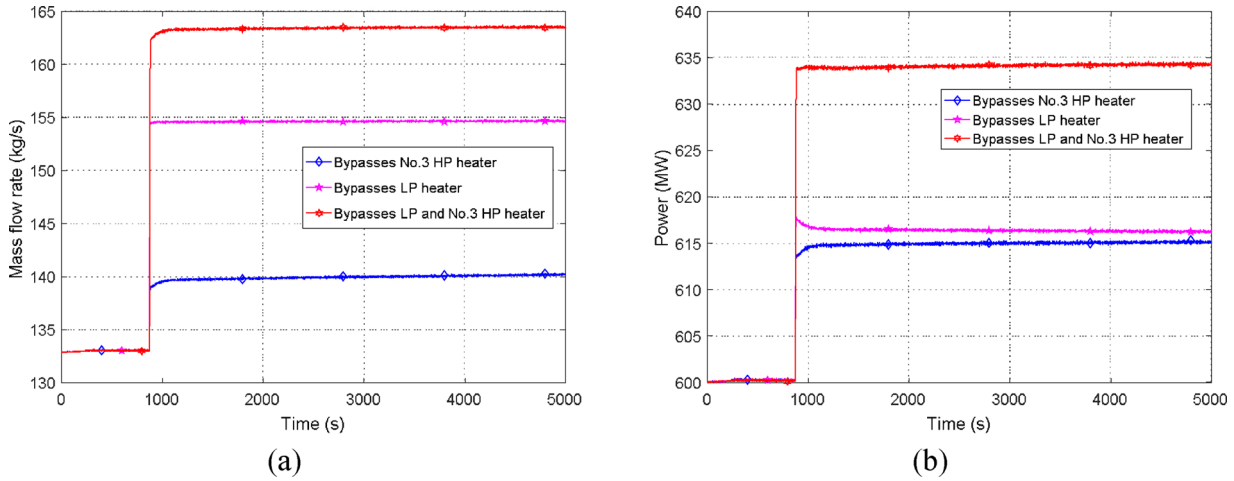

Fig. 13. Using HTTS to heat feed water instead of preheater: (a) Mass flow rate; (b) Output power.

Table 2
Energy and exergy analysis of HTTS charging process.

Generated power (MW)	IPTB inlet enthalpy	IPTB inlet entropy	LPTB inlet enthalpy	LPTB inlet entropy	Extract steam (kg/s)	Stored thermal energy (MW)	Lost exergy (MW)
600	3597.1	7.27	3168.9	7.32	0	0	0
590.4	3597.5	7.315	3209.2	7.36	46.1	19.9	18.52
584.5	3598.4	7.35	3245.6	7.4	83.4	29.42	30.67
580.7	3599.3	7.39	3279.5	7.43	113.7	36.36	37.71
578.2	3598.2	7.41	3306.9	7.46	138.2	40.26	42.32
577.3	3596.8	7.43	3329.3	7.48	158	42.27	44.62
576.5	3595	7.45	3348.1	7.5	174.2	43	45.6

inlet temperature is 838 K. The initial temperature of $LiNO_3$&$NaNO_3$& KCl, LiCl&LiOH, KNO_3, KCl&$ZnCl_2$, and KCl&KF&K_2CO_3 are 410, 510, 580, 680 and 780 K, respectively. It can be assumed that each set of container has same temperature distribution, due to the parallel structure. Therefore, the study of entail HTTS can be simplified as a study of one set of container. After one hours charging, the temperature distributions are presented in Fig. 17. The plotted temperature distribution is the area shaded in Fig. 15.

The stored thermal energy in mass M_{PCM} for a solid-liquid transition in a PCM is calculated by [6]:

$$Q_{storage} = M_{PCM}[c_{p,s}(T_{melting} - T_{solid}) + L + c_{p,l}(T_{liquid} - T_{melting})], \quad (25)$$

where, M_{PCM} is the mass of PCM, $c_{p,s}$ is the heat capacity for solid phase, $c_{p,l}$ is the heat capacity for liquid phase, L is the latent heat, T_{solid} is the solid temperature (initial temperature), T_{liquid} is the liquid temperature (final temperature), and $T_{melting}$ is the phase change temperature.

Based on the above equation, the total stored thermal energy in the HTTS system is 124.7 GJ, in one hour charging process, and 32.1. 20.3. 32.5, 31.7 and 8.1 GJ for $LiNO_3$&$NaNO_3$&KCl, LiCl&LiOH, KNO_3, KCl& $ZnCl_2$, and KCl&KF&K_2CO_3 layers, respectively. Therefore, the average power of the HTTS system is 34.64 MW. The dynamic steam outlet temperature of the five PCM layers are plotted in Fig. 18. It can be seen that the outlet temperature does not change much, in the charging process. This ensures the temperature difference between HTF and PCMs in a reasonable range, and then stabilizes the heat transfer rate during the storage process.

For the other HTTS integrations strategies, the HTF could flow into or out of the HTTS at different positions based on the temperature of HTF and PCMs. For the second HTTS charging strategies, the HTS could bypass PCM1, PCM2 and PCM3, and pass through PCM4 and PCM5. For the third HTTS charging strategy, the HTF could pass through PCM1, PCM2 and PCM3, and then looping back to the LPTB inlet. For the first HTTS discharging strategy, the HTF will pass through entire HTTS from PCM5 to PCM1. For the second HTTS discharging strategy, the HTF will pass through PCM5 or PCM4 or PCM5 and PCM4 depending on different integration methods.

4. Power plant flexible operation in supporting grid frequency modulation

The simulation results show that the power plant could operate with a wider range of power generation variation and increased flexibility through HTTS integration. The HTTS could accumulate or release thermal energy to regulate the plant power output, therefore this offers the enhanced capability in providing the services to load shifting and grid frequency control. This section is to present the results in investigating how the HTTS integration help achieve the improved grid demand responses.

First, the simulation study is conducted to test whether the extra regulation to heat via the HTTS can speed up the power plant dynamic responses. The simulation results are shown in Fig. 19. The solid line is the power output dynamic responses with the integration HTTS in action, in which the output power is regulated with the support of HTTS charging and discharging processes while the amount of feed coal (fuel input) remains the constant. The dashed line represents the power output without HTTS integration and the power output is directly controlled by change the flow rate of coal feeding. It can be seen that the power plant shows faster dynamic responses and gave a more smooth transition with HTTS integration compared with the plant responses without HTTS.

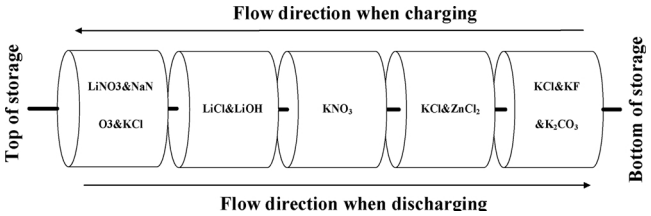

Fig. 14. Designed HTTS model with five PCMs.

Table 4
Thermodynamic properties of salts compositions extracted from [23,24].

Material	Composition, wt%	Melting temperature, ℃	Latent heat, J/g	Specific heat, J/(g·K)		Density, g/cm^3
				Solid	Liquid	
PCM1	KCl(40)- 23KF-37K_2CO_3	528	283	1.00	1.26	2.28
PCM2	KCl (54)- 46 $ZnCl_2$	432	218	0.67	0.88	2.41
PCM3	KNO_3	330	172	1.22	1.22	2.26
PCM4	LiCl(37)-63LiOH	262	485	2.40	2.40	1.55
PCM5	$LiNO_3$(55.4)-4.5$NaNO_3$-40.1KCl	160	266	1.4	1.4	2.21

Table 3
Energy and exergy analysis of HTTS discharging process.

Generated power (MW)	Deaerator outlet enthalpy	Deaerator outlet entropy	LPTB inlet enthalpy	LPTB inlet entropy	Generated steam (kg/s)	Released thermal energy (MW)	Increased exergy (MW)
600	720.9	1.98	3168.9	7.32	0	0	0
620	741.4	2.02	3193.26	7.32	32.2	78.95	28.07
637	759.4	2.06	3212.13	7.308	60.9	149.55	54.26
644.4	762.4	2.07	3219.56	7.305	72.6	178.4	65.08

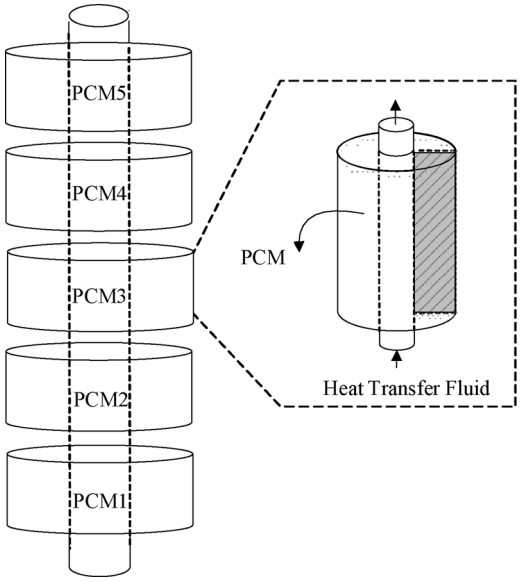

Fig. 15. Structure of single HTTS set.

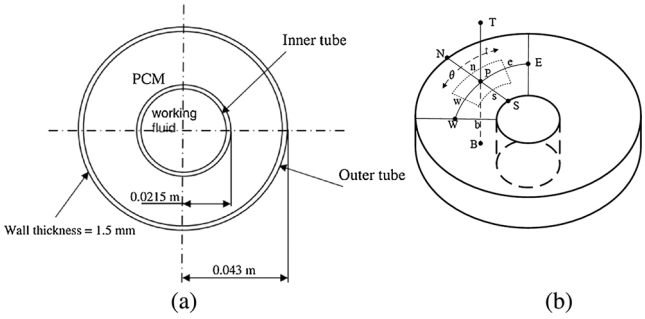

Fig. 16. Structure of one set: (a) configuration and dimensions [25]; (b) three-dimensional heat conduction.

To test the dynamic responses of the power plant in serving grid load balance, a grid frequency response model is built which is then linked to the power plant model. This frequency response system model can represent how the frequency control stabilizes the grid frequency to a steady-state value within the range of frequency deviation allowed by the grid code while load or generation is changed [28]. Due to power plant mechanical inertia, the grid frequency changes will take time

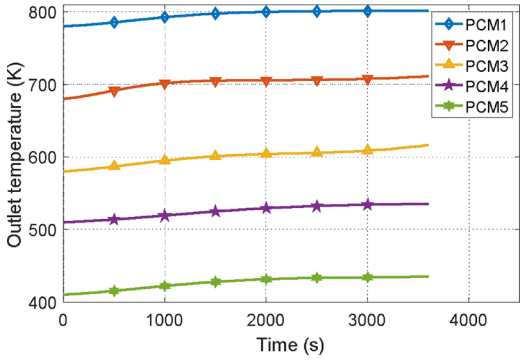

Fig. 18. Outlet temperature of five layers.

when the mismatch happens between the load and the generation. The power plant control will monitor the frequency variations and take the information into its control decision making. When the frequency drops, more power needs to be generated to meet the load demand or vice versa.

The governing equation to the generator speed changes is relevant to the system inertia (J) and torque balance as shown in Eq. (26) [29]:

$$J\frac{d\omega}{dt} = \tau_a = \tau_m - \tau_e, \tag{26}$$

where, ω is the rotation speed, τ_a is the accelerating torque, τ_m is the mechanical torque, and τ_e is the electrical torque. The inertia constant (H) of a synchronous machine can be estimated by [30]:

$$H = \frac{E_{kinetic}}{S_{rated}} = \frac{1}{2}\frac{J\omega^2}{S_{rated}}, \tag{27}$$

where, $E_{kinetic}$ is the kinetic energy of synchronous machine, and S_{rated} is the nominal power rating. The droop constant R_i describes the power versus frequency characteristic of the generator speed governor setting and it is defined as [30]:

$$R_i = -\frac{\Delta f}{f_0}\Big/\frac{\Delta Power_i}{S_i}, \tag{28}$$

where, Δf is the frequency deviation, f_0 is the normal grid frequency, $\Delta Power_i$ is the power deviation of the i-th generation unit, and S_i is the nominal power rating. The imbalance power and the frequency deviation can be describe as [30]:

$$Power_M - Power_L = 2H\frac{d\Delta f}{dt} + D\Delta f, \tag{29}$$

where, $Power_L$ is the load demand, $Power_M$ is the generated power, and D is the load response. Applying Laplace transform to the above equation [31], Eq. (30) can be derived:

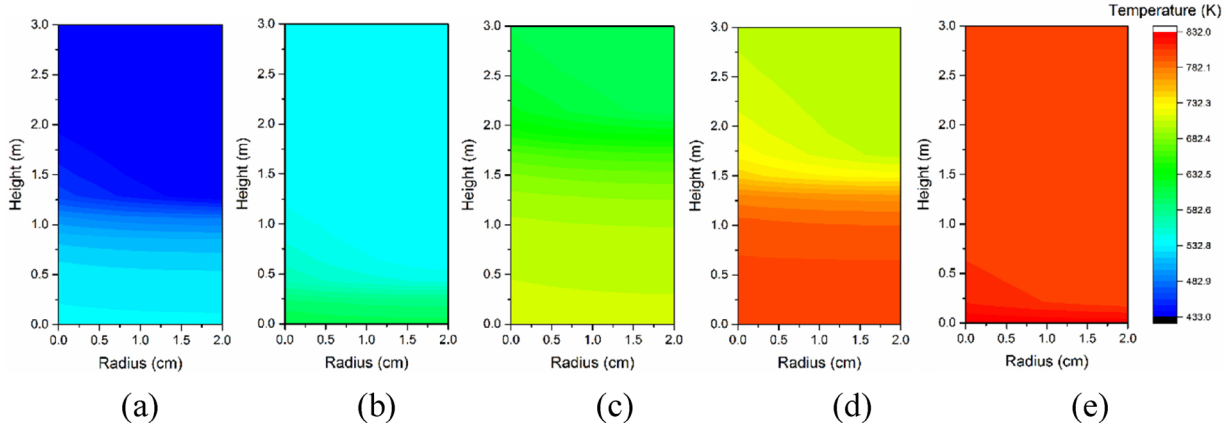

Fig. 17. HTTS temperature.

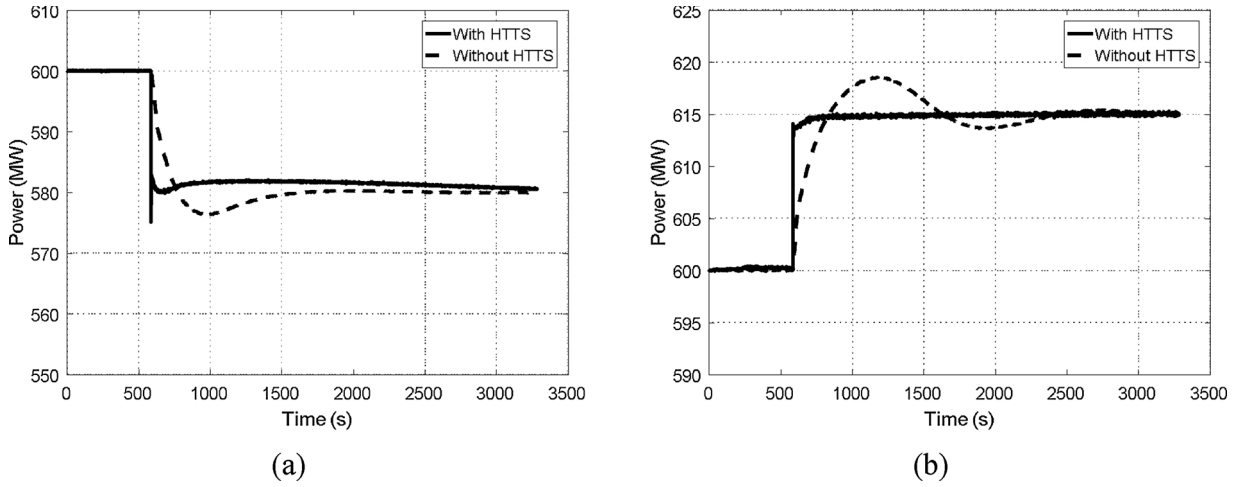

Fig. 19. Contribution of the HTTS to match the load demand: (a) OFF peak period; (b) Peak period.

$$Power_M(s) - Power_L(s) = (2H \times s + D)\Delta f(s). \quad (30)$$

Some assumptions were made based on the GB (Great Britain) power system characteristics. The droop constant (R_i) is set to 4%, the load response (D) is 1. The mechanical acceleration time constant ($M = 2H$) is about 10.8 s.

Fig. 20 shows the model to represent the GB power grid frequency responses, which is used to study the grid frequency regulation if the supercritical coal-fired power plant is required or committed to provide the service to grid frequency control. In Great Britain, the average demand is about 40 G W, and the coal-fired power plants currently provide about 15% [32] of the total load demand around 6 G W. With the model shown in Fig. 20, the simulation study is conducted by link of the grid model to the power plant model responses. Fig. 21 shows the grid frequency response when the load demand decreases 0.5% at the time of 584 s from the time when the simulation starts. The system frequency increases; then the supercritical coal-fired power plants are controlled to decrease the output power to restore the rated frequency of the power grid. It can be seen that from Fig. 21, the frequency response is faster when the supercritical coal-fired power plants are integrated with HTTS.

Fig. 22 shows the grid frequency response after a sudden increase of load demand. The grid frequency starts dropping and the frequency nadir is achieved; then the power plants start to increase its output power, and the grid frequency is brought back to the designed value. From this case, it is clear to see how the system dynamic response speed changes when the HTTS is integrated to the power plant action.

The imbalance of the load demand and power generation leads to frequency deviations; the primary spin reserve from the power plant mechanical inertia could stabilize grid frequency at a certain level, which is called primary frequency control. The secondary frequency

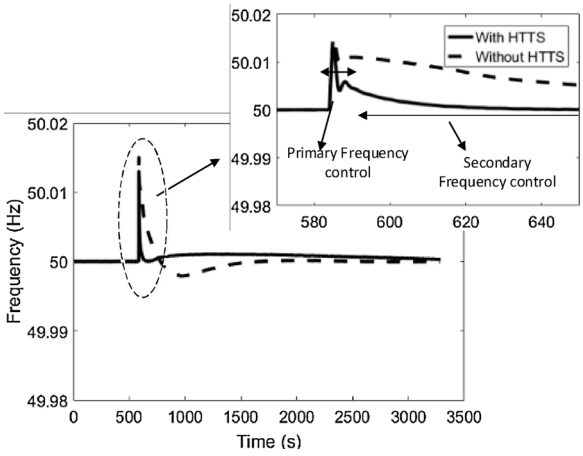

Fig. 21. Grid frequency response for load decrease.

control is needed to recuperate the rated frequency and release the primary reserve. It can be seen from Fig. 19, integrating HTTS into supercritical coal-fired power plant could improve the plant dynamic performance for flexible operation. Figs. 21 and 22 demonstrate the merit of HTTS integration in peak shifting of electrical demand and grid frequency control.

5. Conclusion

This paper describes the modelling and simulation study for HTTS integration into a supercritical coal-fired power plant for efficient and

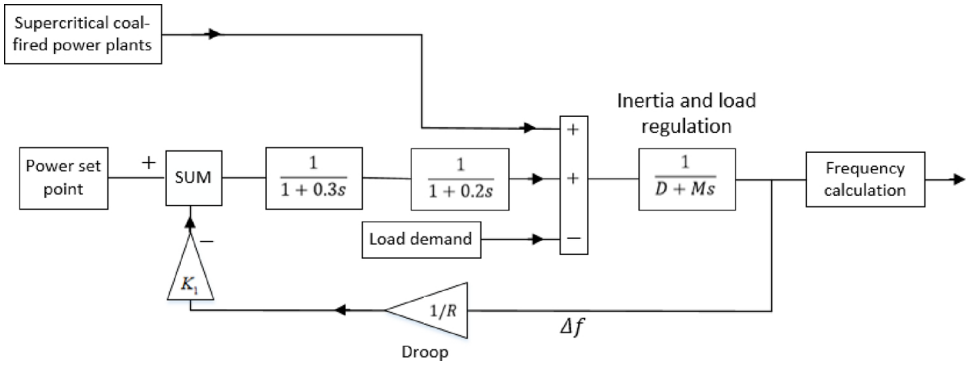

Fig. 20. Block diagram of GB power grid frequency response system.

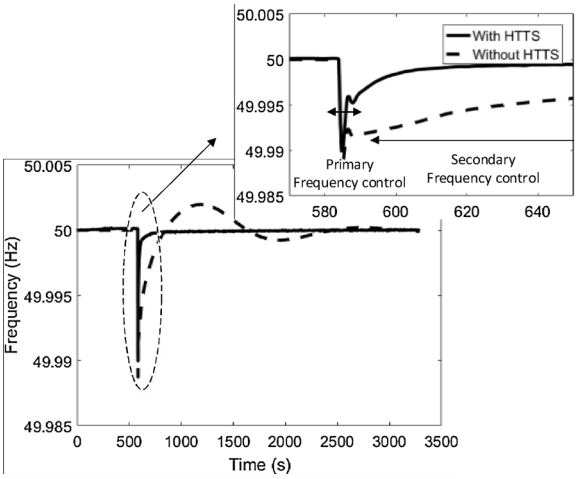

Fig. 22. Grid frequency response for load increase.

flexible plant operation. Three HTTS charging strategies, and two HTTS discharging strategies were investigated. The simulation results show that it is possible to extract thermal energy from water steam cycle for HTTS during the off-peak time period, and the stored thermal energy can be discharged back to the power generation process to water steam loop during the peak demand period to boost the power generation. The HTTS integration steady state simulation results were analysed from the energy and exergy balance point of view. From this study, it is evidenced that:

(1) It is feasible to integrate HTTS into the power plant steam and water loop to regulate the thermal energy release to the power generation process.
(2) In the HTTS charging process, the amount of the steam extraction needs to be restricted to a feasible range in order to maintain a stable power output. For the first HTTS charging strategy, the maximum flow rate of steam extraction from IPTB inlet is 80 kg/s, and the relative reduction of the power output is 13.3%. For the section HTTS charging strategy, the maximum flow rate of stream extraction from LPTB inlet is 56 kg/s, and the relative reduction of the power output is 6.5%. For the third HTTS charging strategy, the maximum flow rate of steam extraction from IPTB inlet is 174 kg/s, and the relative reduction of the power output is 3.9%.
(3) For the first HTTS discharging strategy, the maximum mass flow rate of generated steam is 72.6 kg/s, and the corresponding overall output power is 644.4 MW. For the section HTTS discharging strategy, the maximum output power is 634 MW.
(4) With the HTTS integration, the supercritical coal-fired power plant shows faster dynamic responses to the load demand changes and performs better in grid frequency services.

Acknowledgements

The authors would like to acknowledge the support of the Engineering and Physical Research Council (EPSRC) for their support for the project - Flexible and Efficient Power Plant: Flex-E-Plant (Grant number: EP/K021095/1) and also the grant support from EPSRC (EP/L019469) . We also thank the following partners for their the valuable contributions: GE Energy, Doosan Babcock Limited, Centrica plc., EDF Energy (West Burton Power) Limited., Uniper Technologies Limited, Goodwin Steel Castings Limited, NPL Management Limited, R-MC Power Recovery Limited., RWE Generation UK plc., Scottish and Southern Energy (SSE) plc., Siemens Industrial Turbomachinery, and TWI Limited. The authors wish to thank the China Scholarship Council (CSC) for the PhD scholarship. The authors would like to thank the support from China Nation Basic Research Program 973 (2015CB251301).

References

[1] W. Hausz, B. Berkowitz, R. Hare, Conceptual Design Of Thermal Energy Storage Systems For Near Term Electric Utility Applications, Department of Energy, Office of Energy Technology, Division of Storage Systems, 1978.
[2] T. Nuytten, B. Claessens, K. Paredis, J. Van Bael, D. Six, Flexibility of a combined heat and power system with thermal energy storage for district heating, Appl. Energy 104 (2013) 583–591.
[3] G. Pagliarini, S. Rainieri, Modeling of a thermal energy storage system coupled with combined heat and power generation for the heating requirements of a University Campus, Appl. Therm. Eng. 30 (2010) 1255–1261.
[4] M. Johnson, J. Vogel, M. Hempel, A. Dengel, M. Seitz, B. Hachmann, High temperature latent heat thermal energy storage integration in a co-gen plant, Energy Procedia 73 (2015) 281–288.
[5] A. Koca, H.F. Oztop, T. Koyun, Y. Varol, Energy and exergy analysis of a latent heat storage system with phase change material for a solar collector, Renew. Energy 33 (2008) 567–574.
[6] S. Kuravi, J. Trahan, D.Y. Goswami, M.M. Rahman, E.K. Stefanakos, Thermal energy storage technologies and systems for concentrating solar power plants, Prog. Energy Combust. Sci. 39 (2013) 285–319.
[7] M. Medrano, A. Gil, I. Martorell, X. Potau, L.F. Cabeza, State of the art on high-temperature thermal energy storage for power generation. Part 2—case studies, Renew. Sustain. Energy Rev. 14 (2010) 56–72.
[8] Y. Tian, C.-Y. Zhao, A review of solar collectors and thermal energy storage in solar thermal applications, Appl. Energy 104 (2013) 538–553.
[9] U. Herrmann, D.W. Kearney, Survey of thermal energy storage for parabolic trough power plants, Trans.-Am. Soc. Mechan. Eng. J. Sol. Energy Eng. 124 (2002) 145–152.
[10] D. Li, Y. Hu, W. He, J. Wang, Dynamic modelling and simulation of a combined-cycle power plant integration with thermal energy storage, Automation and Computing (ICAC), 2017 23rd International Conference on, (2017), pp. 1–6.
[11] J.D. Wojcik, J. Wang, Technical feasibility study of thermal energy storage integration into the conventional power plant cycle, Energies 10 (2017) 205.
[12] M. Huebel, C. Gierow, J.H. Prause, S. Meinke, E. Hassel, Simulation of ancillary services in thermal power plants in energy systems with High impact of renewable energy, ASME 2017 Power Conference Joint With ICOPE-17 Collocated With the ASME 2017 11th International Conference on Energy Sustainability, the ASME 2017 15th International Conference on Fuel Cell Science, Engineering and Technology, and the ASME 2017 Nuclear Forum, (2017) pp. V002T08A008-V002T08A008.
[13] C. Wang, Y. Zhao, M. Liu, Y. Qiao, D. Chong, J. Yan, Peak shaving operational optimization of supercritical coal-fired power plants by revising control strategy for water-fuel ratio, Appl. Energy 216 (2018) 212–223.
[14] Y. Zhao, C. Wang, M. Liu, D. Chong, J. Yan, Improving operational flexibility by regulating extraction steam of high-pressure heaters on A 660 MW supercritical coal-fired power plant: a dynamic simulation, Appl. Energy 212 (2018) 1295–1309.
[15] B. Tashtoush, M. Molhim, M. Al-Rousan, Dynamic model of an HVAC system for control analysis, Energy 30 (2005) 1729–1745.
[16] S. Quoilin, R. Aumann, A. Grill, A. Schuster, V. Lemort, H. Spliethoff, Dynamic modeling and optimal control strategy of waste heat recovery organic rankine cycles, Appl. Energy 88 (2011) 2183–2190.
[17] M. Draganescu, S. Guo, J. Wojcik, J. Wang, X. Liu, G. Hou, et al., Generalized predictive control for superheated steam temperature regulation in a supercritical coal-fired power plant, CSEE J. Power Energy Syst 1 (2015) 69–77.
[18] S. Guo, Model Based Analysis of Power Plant Integrated with a Post Combustion Carbon Capture Process, University of Warwick, 2015.
[19] M. Draganescu, Study of Supercritical Coal-Fired Power Plant Dynamic Responses and Control for Grid Code Compliance, University of Warwick, 2015.
[20] M. Ameri, P. Ahmadi, A. Hamidi, Energy, exergy and exergoeconomic analysis of a steam power plant: a case study, Int. J. Energy Res. 33 (2009) 499–512.
[21] I.H. Aljundi, Energy and exergy analysis of a steam power plant in Jordan, Appl. Therm. Eng. 29 (2009) 324–328.
[22] P.C. Bergman, A. Boersma, R. Zwart, J. Kiel, Torrefaction for Biomass Co-Firing in Existing Coal-Fired Power Stations, Energy Centre of Netherlands, 2005 Report No. ECN-C-05-013.
[23] F. Agyenim, N. Hewitt, P. Eames, M. Smyth, A review of materials, heat transfer and phase change problem formulation for latent heat thermal energy storage systems (LHTESS), Renew. Sustain. Energy Rev. 14 (2010) 615–628.
[24] M.M. Kenisarin, High-temperature phase change materials for thermal energy storage, Renew. Sustain. Energy Rev. 14 (2010) 955–970.
[25] K. Lafdi, O. Mesalhy, A. Elgafy, Graphite foams infiltrated with phase change materials as alternative materials for space and terrestrial thermal energy storage applications, Carbon 46 (2008) 159–168.
[26] S. Patankar, Numerical Heat Transfer and Fluid Flow, CRC press, 1980.
[27] P. Verma, S. Singal, Review of mathematical modeling on latent heat thermal energy storage systems using phase-change material, Renew. Sustain. Energy Rev. 12 (2008) 999–1031.
[28] F. Díaz-González, M. Hau, A. Sumper, O. Gomis-Bellmunt, Participation of wind power plants in system frequency control: review of grid code requirements and control methods, Renew. Sustain. Energy Rev. 34 (2014) 551–564.
[29] W. Murrell, L. Ran, J. Wang, Modelling UK power system frequency response with increasing wind penetration, 2014 IEEE Innovative Smart Grid Technologies-Asia (ISGT ASIA), (2014), pp. 1–6.

[30] V. Knap, S.K. Chaudhary, D.-I. Stroe, M. Swierczynski, B.-I. Craciun, R. Teodorescu, Sizing of an Energy Storage System for Grid Inertial Response and Primary Frequency Reserve, (2016).
[31] Y. Huang, G. Mu, L. Li, G. Yan, J. Liu, Z. Wang, Method of obtaining the sensitive disturbances of frequency control system including AGC by analyzing the frequency-response trajectory, IEEE PES Innovative Smart Grid Technologies, (2012), pp. 1–5.
[32] E. I. S. Department for Business, Digest of UK energy statistics, Energy and Climate Change: Evidence and Analysis, (2017).